

FURTHER STUDIES OF UNDULATOR TAPERING IN X-RAY FELs

Alan Mak*, Francesca Curbis, Sverker Werin, MAX IV Laboratory, Lund University, Sweden

Abstract

We further the studies of the model-based optimization of tapered free-electron lasers presented in a recent publication [Phys. Rev. ST Accel. Beams **18**, 040702 (2015)]. Departing from the ideal case, wherein the taper profile is a smooth and continuous function, we consider the more realistic case, with individual undulator segments separated by break sections. Using the simulation code GENESIS, we apply our taper optimization method to a case, which closely resembles the FLASH2 facility in Hamburg, Germany. By comparing steady-state and time-dependent simulations, we examine how time-dependent properties alter the optimal taper scenario. From the simulation results, we also deduce that the “traditional” empirical method, whereby the intermediate radiation power is maximized after closing every undulator gap, does not necessarily produce the highest final power at the exit of the undulator line.

INTRODUCTION

Present-day imaging experiments at x-ray free-electron laser (FEL) facilities call for an increased number of photons within a shorter pulse duration [1, 2]. To meet the stringent demand on the radiation power, the technique of undulator tapering has been revisited in recent years, and much theoretical effort has been dedicated to the optimization of this technique [3–6].

In a recent publication [6], we propose a modification to the Kroll-Morton-Rosenbluth (KMR) model [7], which serves as a method of optimizing the taper profile. The method features a variable phase of the resonant particle, and opens up possibilities for further enhancement of radiation power beyond the constant-phase model.

In the ideal case, the taper profile $K(z)$ is a smooth and continuous function. However, most existing taperable x-ray FELs, such as FLASH2 [8] and SACLA [9], consist of individual undulator segments separated by break sections. With these limitations, a reduction of radiation power from the ideal case is inevitable.

The break sections are needed for beam focusing, trajectory correction and diagnostics. However, vacuum diffraction of the optical beam in the break sections leads to a decrease in the on-axis field strength, which also causes particle detrapping [3].

Also, as each undulator segment is uniform within itself, the segment length sets a limit on the rate at which K can decrease, and hence a limit on the bucket deceleration rate. Furthermore, if the segment length is larger than the synchrotron period, the electron beam can absorb energy momentarily from the optical beam [6].

In this article, we study a case with 2.5-m undulator segments separated by break sections. Using the simulation code GENESIS [10], we adapt our taper optimization method to these limitations, and obtain the highest possible power. We then compare the simulation results obtained in the steady-state mode and the time-dependent mode, quantifying the effects of time-dependent properties.

The case chosen for our simulation studies is intended to match the design parameters of the FLASH2 facility, which achieved its first lasing [11] in August 2014.

CASE DEFINITION

For the simulation studies in this article, we choose a case with main parameters as shown in Table 1. These parameter values are within the designed range for the FLASH2 facility [8].

Table 1: Main Parameters for the Simulated Case

Parameter	Symbol	Value
Electron beam energy	E	1.25 GeV
Peak current	I	2.5 kA
Bunch charge	Q	630 pC
Bunch length	σ_t	30 μ m
Energy spread	σ_E	0.5 MeV
Normalized emittance	$\varepsilon_{x,y}$	1.4 μ m rad
Average beta function	$\langle\beta_{x,y}\rangle$	6 m
Radiation wavelength	λ	6 nm
Undulator period	λ_w	31.4 mm
Undulator segment length	L_{seg}	2.5 m

The undulator segments considered in this case are planar. The lattice for the transverse focusing of the electron beam is in a FODO configuration. The period of the FODO cell is 6.6 m, in which two quadrupole magnets are 3.3 m apart from one another.

The FLASH2 facility has 12 undulator segments [8]. But in our simulation studies, we first consider a total of 30 segments, for the purpose of understanding the FEL dynamics over a long distance. After that, we consider the more realistic 12-segment case, by discarding all the subsequent segments in the simulations.

TAPER OPTIMIZATION METHOD

Our taper optimization method is detailed in a recent publication [6]. The method is based on the KMR model [7] and a modification thereto. It considers a resonant particle with phase-space coordinates (ψ_R, γ_R) . With a constant phase $\psi_R(z) = \psi_R(0)$, it is known as the ordinary KMR

* alan.mak@maxlab.lu.se

method. With an increasing phase

$$\psi_R(z) = \frac{\pi}{2} \left(\frac{z}{L_d} \right)^n,$$

it is known as the modified KMR method, where L_d and n are positive real numbers at our choice.

L_d is known as the detrapping length. At $z = L_d$, the phase ψ_R reaches $\pi/2$. The area of ponderomotive bucket then becomes zero, and total detrapping occurs. Adjusting L_d allows us to control the rate at which ψ_R increases.

The degree n does not have to be an integer. But in Ref. [6], we have shown with another case that the output power is maximized by choosing $n = 1$. In this article, we restrict ourselves to $n = 1$.

The method involves iterative simulations, with step size Δz along the undulator line. In the ideal case, Δz should be as small as possible, such as $\Delta z = \lambda_w$. But in the case at hand, the individual undulator segments require us to make the adaptation $\Delta z = L_{\text{seg}}$. Furthermore, we adapt the method to the presence of break sections. In each step Δz , the decrease in on-axis field amplitude due to vacuum diffraction in the preceding break section is taken into account.

The iterative simulations are performed in the steady-state mode of GENESIS. Upon choosing a constant resonant phase ψ_R for the ordinary KMR method or a detrapping length L_d for the modified KMR method, the iterative simulations will result in a taper profile $K(z)$. Upon obtaining the taper profile, we input it to GENESIS again and run it in the time-dependent mode.

RESULTS AND DISCUSSIONS

General Results with 30 Undulator Segments

To examine the FEL dynamics over a long distance, we simulate a total of 30 undulator segments with GENESIS.

For the ordinary KMR method, we vary the resonant phase ψ_R from 0.05 rad to 0.5 rad at intervals of 0.05 rad. For the modified KMR method, we vary the detrapping length L_d from 50 m to 500 m at intervals of 50 m.

In all these runs, we probe the final radiation power at the exit of the 30th undulator segment. The results are summarized in Fig. 1. The blue solid curves are the results of steady-state simulations, and the green dashed curves are the results of time-dependent simulations.

Ordinary KMR versus Modified KMR In the steady-state mode (see blue solid curves in Fig. 1), the final power is maximized at $\psi_R = 0.35$ rad for the ordinary KMR method, and at $L_d = 200$ m for the modified KMR method. The maximized final powers are 76.8 GW and 94.9 GW, respectively. The maximized final power for the modified KMR method is 123% that for the ordinary KMR method.

In the time-dependent mode (see green dashed curves in Fig. 1), the final power is maximized at $\psi_R = 0.2$ rad for the ordinary KMR method, and at $L_d = 300$ m for the modified KMR method. The maximized final powers are 18.9 GW and 21.4 GW, respectively. The maximized final power for

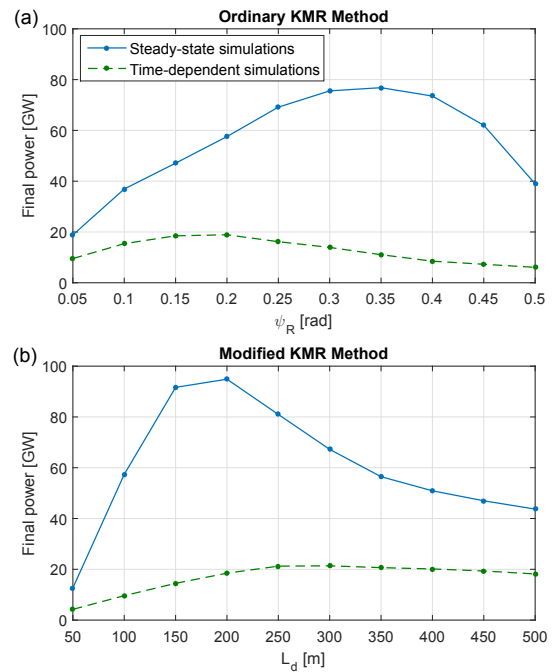


Figure 1: The final radiation power at the exit of the 30th undulator segment (a) as a function of the resonant phase ψ_R in the ordinary KMR method and (b) as a function of the detrapping length L_d in the modified KMR method. The blue solid curves are the results of steady-state simulations, and the green dashed curves are the results of time-dependent simulations.

the modified KMR method is 113% that for the ordinary KMR method.

In both the steady-state and the time-dependent modes, the modified KMR method produces a higher final power than the ordinary KMR method. This shows that an increasing ψ_R is more favourable than a constant ψ_R for maximizing the final power, even when time-dependent properties are taken into account. The benefit of using an increasing ψ_R over a constant ψ_R has been justified in Ref. [6] in terms of the initial capturing of particles and the rate of bucket deceleration.

Steady-state versus Time-dependent For the ordinary KMR method [see Fig. 1(a)], the maximized final power in the time-dependent mode constitutes a 75% drop from that in the steady-state mode. For the modified KMR method [see Fig. 1(b)], the maximized final power in the time-dependent mode constitutes a 77% drop from that in the steady-state mode. These show that time-dependent properties are a significant cause of power reduction.

The power reduction can be understood as follows. In GENESIS, a steady-state simulation is equivalent to considering only the central slice in a time-dependent simulation. Thus, a taper profile $K(z)$ obtained in the steady-state mode is only optimal for the centremost part of the longitudinal bunch profile, when running in the time-dependent mode. Towards the head and the tail of a Gaussian bunch profile,

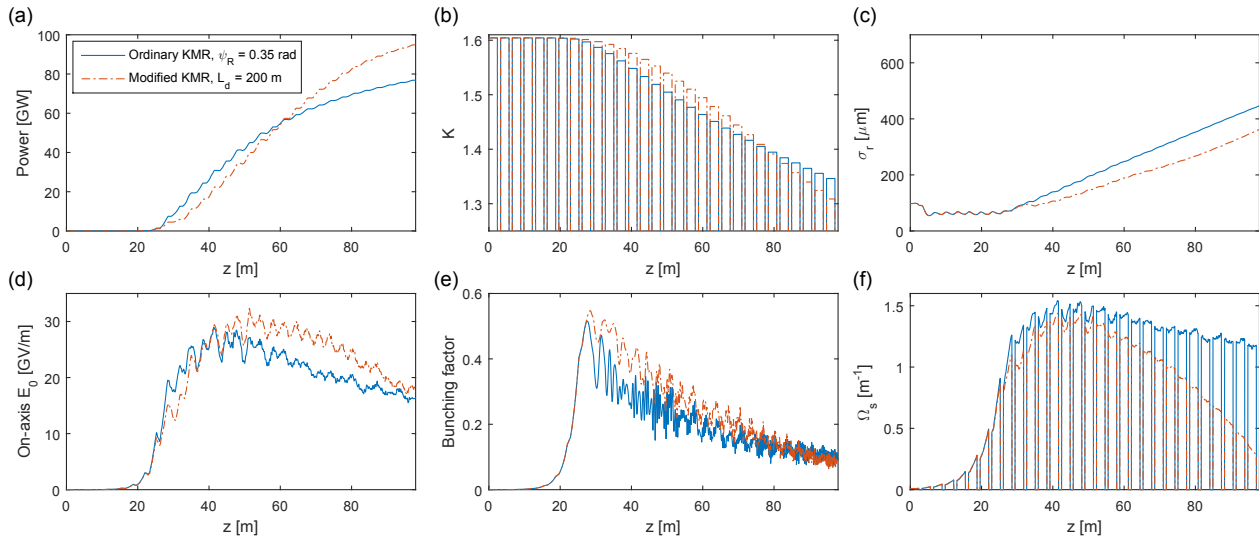


Figure 2: Results of steady-state simulations, showing the optimal scenarios of the ordinary KMR method (blue) and the modified KMR method (red) with the use of 30 undulator segments. The following quantities are plotted as functions of the distance z along the undulator line: (a) the radiation power; (b) the undulator parameter K ; (c) the rms radius of the optical beam; (d) the field amplitude on axis; (e) the bunching factor; (f) the synchrotron frequency.

the slice current is significantly lower. These parts of the bunch behave in a non-optimal fashion under a taper profile $K(z)$ optimized for the central slice, thus reducing the average power produced by the bunch.

Another observation is that the optimal scenarios are not the same in the steady-state mode and in the time-dependent mode. When going from steady-state to time-dependent in the ordinary KMR method, the optimal ψ_R decreases. Similarly, when going from steady-state to time-dependent in the modified KMR method, the optimal L_d increases, which corresponds to an overall decrease in the range of ψ_R .

As discussed in Ref. [6], the area of the ponderomotive bucket decreases with ψ_R , while the bucket deceleration rate increases with ψ_R . This implies that in the presence of time-dependent effects, it is preferable to maintain a relatively large bucket at the expense of slowing down the bucket deceleration. This trade-off can be justified by the fact that time-dependent effects constitute an additional source of particle detrapping [3].

Optimal scenarios with 30 Segments

Without any tapering, power saturation occurs at around $z = 30$ m in the 10th undulator segment. This is known as the initial saturation point. The saturation power is 2.5 GW in the steady-state mode and 1.7 GW in the time-dependent mode.

The optimal taper scenarios in the steady-state mode are examined in Fig. 2. The blue solid curves correspond to the ordinary KMR method with $\psi_R = 0.35$ rad, while the red dashed curves correspond to the modified KMR method with $L_d = 200$ m.

Figure 2(a) shows the evolution of the radiation power along the undulator line. At the exit of the undulator line, the modified KMR method yields a higher power than the

ordinary KMR method does, in agreement with Fig. 1. But upstream at $z = 30 - 60$ m, the situation is actually the opposite, i.e. the modified KMR method gives a *lower* power. This shows that it is possible to obtain a higher power downstream by sacrificing the power upstream. In other words, the “traditional” empirical method, whereby the radiation power is maximized after closing every undulator gap, does not necessarily yield the highest power at the end of the undulator line.

Figure 2(b) shows the taper profiles obtained from the iterative simulations. The individual undulator segments and the break sections are clearly seen. For both the ordinary KMR method and the modified KMR method, the K value hardly changes within the first seven segments. The decrease in K begins slightly before the initial saturation point. Immediately after the initial saturation point, the particle trapping development region begins [3]. In this region, the K value for the modified KMR method decreases more slowly than that for the ordinary KMR method. Downstream in the undulator line, the K value for the modified KMR method decreases more rapidly than that for the ordinary KMR method. Note that the rate of K decrease reflects the rate of bucket deceleration. For the modified KMR method, the bucket deceleration is kept slow in the particle trapping development region, thus allowing more particles to be captured in the bucket for the subsequent energy extraction.

Figure 2(c) shows the optical beam size as a function of z . Before the initial saturation point ($z = 30$ m), gain guiding keeps the optical beam size small. Beyond the initial saturation point, gain guiding is weakened, and refractive guiding becomes dominant. The strength of refractive guiding varies with the phase ψ_R as $\cos \psi_R$ [6]. For the modified KMR method, ψ_R increases with z , making the refractive guiding stronger. This partly explains why the optical beam size is

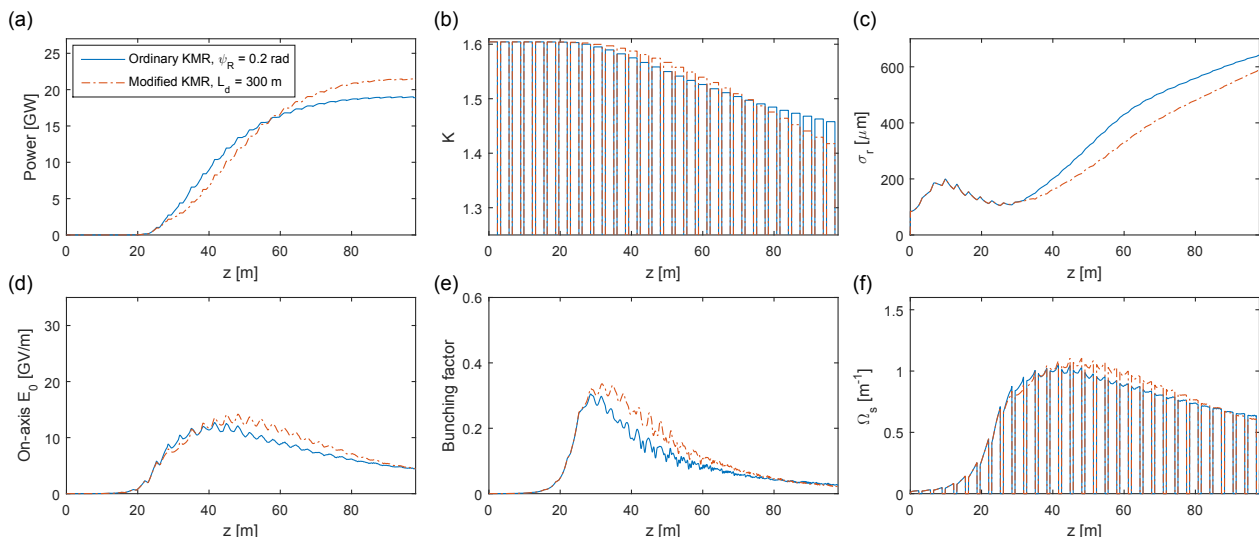


Figure 3: Results of time-dependent simulations, showing the optimal scenarios of the ordinary KMR method (blue) and the modified KMR method (red) with the use of 30 undulator segments. The following quantities are plotted as functions of z : (a) the radiation power; (b) the undulator parameter K ; (c) the rms radius of the optical beam; (d) the field amplitude on axis; (e) the bunching factor; (f) the synchrotron frequency. These quantities are averaged over the electron bunch, and weighted by the slice current.

smaller for the modified KMR method than for the ordinary KMR method beyond the initial saturation point.

The effect of keeping the optical beam size small is also seen in Fig. 2(d), which shows the evolution of the on-axis field amplitude. With a smaller optical beam size beyond the initial saturation point, the modified KMR method gives a stronger field on axis.

Figure 2(e) shows the bunching factor as a function of z . Here the bunching factor is defined as the absolute value of $\langle e^{-i\psi} \rangle$, where the brackets denote the average over all particles, and ψ is the particle phase in the ponderomotive potential. In the particle trapping development region immediately beyond $z = 30$ m, the bunching factor for the modified KMR method is higher than that for the ordinary KMR method. This can be attributed to the larger on-axis field amplitude and the slower decrease in K value.

Figure 2(f) shows the synchrotron frequency as a function of z . The synchrotron frequency is given by [6, 12]

$$\Omega_s(z) = \sqrt{\frac{2\pi e}{m_e c^2 \lambda_w} \frac{K(z) f_B(z) E_0(z)}{\gamma_R^2(z)} \cos[\psi_R(z)]}.$$

For both the ordinary KMR method and the modified KMR method, the synchrotron frequency increases from zero at the entrance to the undulator line and reaches its maximum value slightly after the initial saturation point. Afterwards, the ordinary KMR method exhibits a relatively uniform synchrotron frequency, while the modified KMR method shows a rapid decrease in synchrotron frequency. The behaviour of the synchrotron frequency is a combined effect of the variations in K , E_0 and ψ_R along the undulator line.

Figure 3 shows the corresponding results in the time-dependent mode. The radiation power, K parameter, optical

beam size, on-axis field amplitude and the bunching factor exhibit mostly the same patterns as in Fig. 2. However, the radiation power is lower overall [see Fig. 3(a)]. The diffraction of the optical beam is stronger [see Fig. 3(c)], and the on-axis field weaker [see Fig. 3(d)]. The bunching factor is also smaller overall [see Fig. 3(e)].

In the two optimal taper profiles Fig. 3(b), K decreases more slowly than in their steady-state counterparts [see Fig. 2(b)]. This also shows that in the presence of time-dependent effects, a slower deceleration of the ponderomotive bucket is preferable.

Comparing Fig. 3(f) to Fig. 2(f), we see that time-dependent effects give rise to a different behaviour of the synchrotron frequency. At $z = 40$ – 80 m, the synchrotron frequency is higher for the modified KMR method than for the ordinary KMR method in the time-dependent mode, but the situation is the opposite in the steady-state mode. Also, while the synchrotron frequency for the modified KMR method decreases very rapidly in the steady-state mode, it remains relatively uniform in the time-dependent mode.

Figure 4 shows the the spectral power distributions at the exit of the 30th undulator segment. The blue and red curves correspond to, respectively, the ordinary KMR method with $\psi_R = 0.2$ rad and the modified KMR method with $L_d = 300$ m, which are the the optimal scenarios in the time-dependent mode. The two distributions are largely similar.

Considering Only 12 Segments

The case studied in this article is intended to resemble the FLASH2 facility as closely as possible. The actual FLASH2 facility has 12 undulator segments [8]. Therefore, we now consider the more realistic 12-segment case by discarding all the subsequent segments in our simulation results.

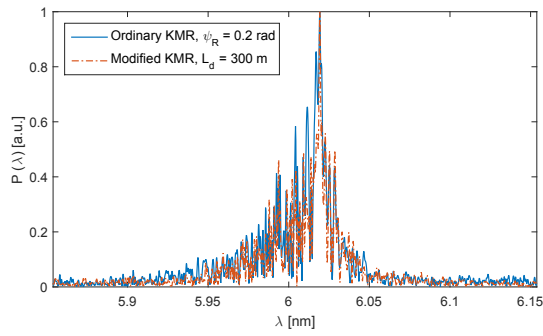


Figure 4: The spectral power distributions for the ordinary KMR method with $\psi_R = 0.2$ rad (blue) and for the modified KMR method with $L_d = 300$ m (red).

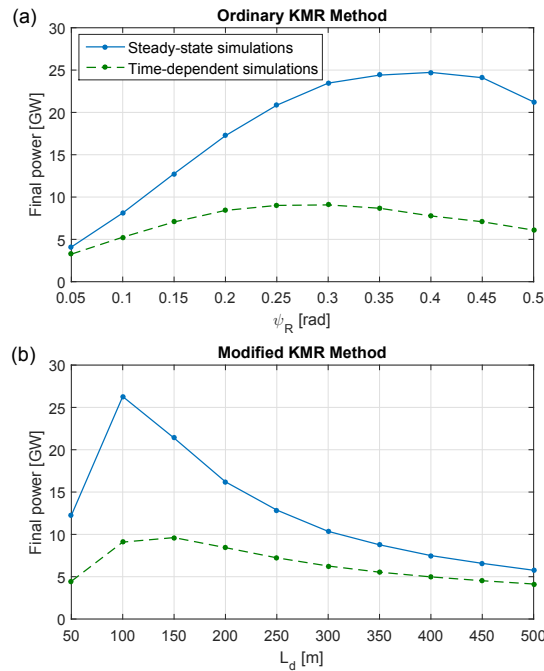


Figure 5: The final radiation power at the exit of the 12th undulator segment (a) as a function of the resonant phase ψ_R in the ordinary KMR method and (b) as a function of the detrapping length L_d in the modified KMR method. The blue solid curves are the results of steady-state simulations, and the green dashed curves are the results of time-dependent simulations.

The final power at the exit of the 12th segment is shown in Fig. 5 for different ψ_R and L_d values. With only 12 segments, the optimal ψ_R and L_d values are, of course, different from those in the 30-segment case. The reason is explained in Ref. [6].

In the steady-state mode (see blue solid curves in Fig. 5), the optimal ψ_R is 0.4 rad, which gives a final power of 24.7 GW; the optimal L_d is 100 m, which gives a final power of 26.3 GW.

In the time-dependent mode (see green dashed curves in Fig. 5), the optimal ψ_R is 0.3 rad, which gives a final power

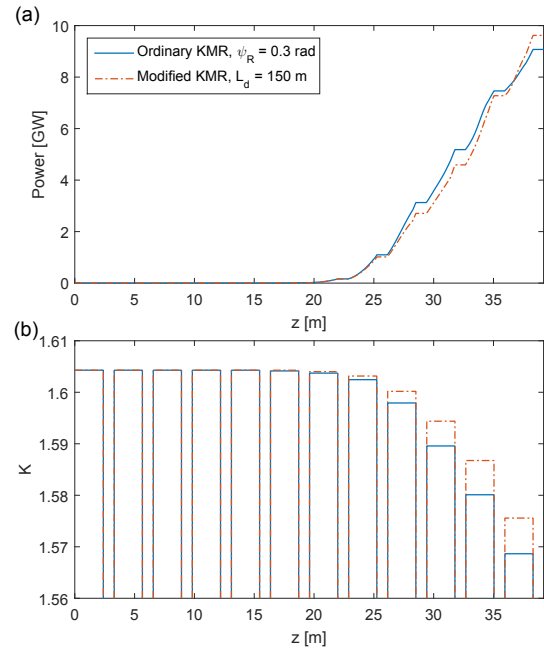


Figure 6: Results of time-dependent simulations, showing the optimal scenarios of the ordinary KMR method (blue) and the modified KMR method (red) with the use of only 12 undulator segments. (a) The bunch-averaged radiation power and (b) the undulator parameter K are plotted as functions of z .

of 9.1 GW; the optimal L_d is 150 m, which gives a final power of 9.6 GW.

With only 12 undulator segments, there is not a huge difference in final power between the ordinary KMR method and the modified KMR method. But compared to the case of no taper, the optimized tapers increase the final power by almost a factor of 11 in the steady-state mode, and a factor of 6 in the time-dependent mode.

The optimal scenarios in the time-dependent mode are shown in Fig. 6. It is apparent from Fig. 6(b) that the K value hardly changes in the first seven undulator segments. The post-saturation power growth is mainly due to the tapering of the last five segments.

As seen from Fig. 6(a), the modified KMR method yields a slightly higher final power at the exit of the 12th segment, compared to the ordinary KMR method. Nonetheless, upstream at $z = 25 - 35$ m, the power produced by the modified KMR method is actually *lower*. Once again, this shows that a higher power can be obtained at the exit of the undulator line by sacrificing the intermediate power upstream. This also implies that the “traditional” empirical method, whereby the intermediate power is maximized after closing every undulator gap, does not necessarily yield the highest final power.

SUMMARY AND OUTLOOK

In this article, we have furthered the study of a previously presented [6] taper optimization method, by adapting the

method to individual undulator segments separated by break sections. Using the simulation code GENESIS [10], we have applied the method to an x-ray FEL case, which closely resembles the FLASH2 facility [8] in Hamburg, Germany. By comparing the simulation results in the steady-state mode and the time-dependent mode, we have quantified the effects of time-dependent properties on the FEL dynamics. It would be an interesting experiment to test the 12-segment time-dependent simulation results on the FLASH2 facility.

REFERENCES

- [1] R. Neutze et al., “Potential for Biomolecular Imaging with Femtosecond X-Ray Pulses”, *Nature* **406**, 752 (2000).
- [2] H. N. Chapman et al., “Femtosecond Diffractive Imaging with a Soft-X-Ray Free-Electron Laser”, *Nature Physics* **2**, 839 (2006).
- [3] Y. Jiao et al., “Modeling and Multidimensional Optimization of a Tapered Free Electron Laser”, *Phys. Rev. ST Accel. Beams* **15**, 050704 (2012).
- [4] C. Emma et al., “Terawatt X-Ray Free-Electron-Laser Optimization by Transverse Electron Distribution Shaping”, *Phys. Rev. ST Accel. Beams* **17**, 110701 (2014).
- [5] E. Schneidmiller, M. Yurkov, “Optimization of a High Efficiency Free Electron Laser Amplifier”, *Phys. Rev. ST Accel. Beams* **18**, 030705 (2015).
- [6] A. Mak, F. Curbis, S. Werin, “Model-Based Optimization of Tapered Free-Electron Lasers”, *Phys. Rev. ST Accel. Beams* **18**, 040702 (2015).
- [7] N. M. Kroll, P. L. Morton, M. N. Rosenbluth, “Free-Electron Lasers with Variable Parameter Wigglers”, *IEEE J. Quantum Electronics* **17**, 1436 (1981).
- [8] K. Honkavaara et al., “Status of the FLASH II Project”, in *Proceedings of the 34th International Free-Electron Laser Conference*, Nara, Japan, 381 (2012).
- [9] T. Ishikawa et al., “A Compact X-Ray Free-Electron Laser Emitting in the Sub-Ångström Region”, *Nature Photonics* **6**, 540 (2012).
- [10] S. Reiche, “GENESIS 1.3: a Fully 3D Time-Dependent FEL Simulation Code”, *Nucl. Instrum. Meth. A* **429**, 243 (1999).
- [11] S. Schreiber, B. Faatz, “First Lasing at FLASH2”, in *Proceedings of the 36th International Free-Electron Laser Conference*, Basel, Switzerland, 7 (2014).
- [12] D. Prosnitz, A. Szoke, V. K. Neil, “High-Gain, Free-Electron Laser Amplifiers: Design Considerations and Simulation”, *Phys. Rev. A* **24**, 1436 (1981).